 https://doi.org/10.3311/PPci.20833

Periodica Polytechnica Civil Engineering, 67(1), pp. 308–324, 2023

Simplified and Cost-Effective Method of Studying the Effect of Steel Fibers on Ultra-high Performance Concrete Specimens' Properties/Members' Performance

Abutu Simon John Smith[1], Gang Xu[1*]

[1] College of Civil Engineering and Architecture, China Three Gorges University, Yichang, 443002, China
[*] Corresponding author, e-mail: xg@ctgu.edu.cn

Received: 16 July 2022, Accepted: 15 November 2022, Published online: 15 December 2022

Abstract

This research work, which presents a simplified technique of modelling steel fibers, uses python algorithm that can be directly run in ABAQUS to automatically generate the location and orientation of steel fibers in a rectangular ultra-high performance concrete specimen, so that the effect of steel fibers on the properties of such a specimen can be directly investigated through numerical simulation. This method is fast, can be applied to structural members of bigger dimensions (like beams, columns, slabs) unlike the existing methods that are only applicable to small size specimens, and also solves the problem associated with previous methods where some fibers may be generated and placed outside the boundary of a specimen, leading to the discard and regeneration of those fibers. To assess the validity of this method, experiments were conducted on the compressive properties of three ultra-high performance concrete cube specimens and the shear performance of two ultra-high performance concrete beams, and the results were compared with the ones obtained using this method. Results indicate over 97% agreement between the experiment and the numerical simulation in ultimate compression force and shear resistance at shear crack and ultimate load phases. The comparison also reveals perfect agreement in the failure mode and crack pattern of the specimens.

Keywords

compression properties, modelling technique, numerical simulation, shear performance, steel fiber, ultra-high performance concrete

1 Introduction

Steel fiber is simply described as a reasonably small discrete steel element with short length and diameter, having aspect ratio (i.e., length to diameter ratio) that ranges from 20 to 100, and may be in any of the several cross-sections that can be easily and randomly dispersed in fresh concrete mix [1]. Studies on incorporating steel fibers into concrete initially started as a method of preventing/controlling plastic and drying shrinkage in concrete [2], and also as a means of tackling the problem of the cost of stirrup installation; as well as the difficulty of placing fresh concrete in a beam with closely-spaced stirrups [3]. These studies led to the development of fiber-reinforced concrete which gained popularity in the early 1960s due to its application in the concrete industry [4]. Over the years, the use of randomly oriented steel fibers in concrete has been reported to improve the tensile strength [5] and the shear strength of concrete [6], prompting ACI Committee 318 [7] to allow the use of deformed steel fibers in place of minimum stirrup reinforcement in its code. Steel fibers are of different types as can be seen in Fig. 1 but the most commonly used types in concrete are straight, crimped, hooked end, twisted and stranded types.

The primary reason for introducing steel fibers into ultra-high performance concrete (UHPC) mix is to improve its toughness [8] and ductility property through matrix

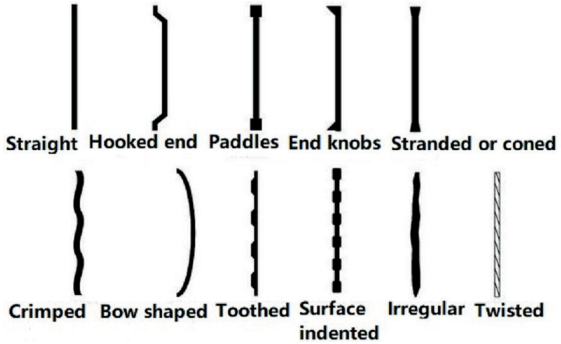

Fig. 1 Type of steel fibers

Cite this article as: Smith, A. S. J., Xu, G. "Simplified and Cost-Effective Method of Studying the Effect of Steel Fibers on Ultra-high Performance Concrete Specimens' Properties/Members' Performance", Periodica Polytechnica Civil Engineering, 67(1), pp. 308–324, 2023. https://doi.org/10.3311/PPci.20833

reinforcement of the part of UHPC specimen or member affected by micro crack formation, in order to minimize the damage that may result from the micro crack formation and subsequent widening [9]. This minimization of the damages resulting from micro crack formation has been reported to improve the post-peak behavior of UHPC specimens subjected to compression loading [10]. In terms of UHPC members' performance, it has been reported that the presence of steel fibers in UHPC members like beam delays crack appearance and propagation [11], changes crack patterns, and also minimizes crack width widening [9], which can eventually lead to the improvement of shear and flexural capacity of the beam as existing studies [12, 13] have shown that the addition of steel fibers in concrete results in a substantial increase in the concrete's ultimate shear strength. For instance, Narayanan and Darwish [14] reported that the addition of 1% volume of steel fibers in a concrete beam led to 170% increase in its ultimate shear strength when compared to that without steel fibers. The presence of steel fibers in UHPC is mostly described in terms of volume fraction, but studies are also conducted on the use of different types of steel fibers as well as different aspect ratios in UHPC mix. Existing literatures [15–18] have shown that some researchers even write UHPC as ultra-high performance fiber reinforced concrete (UHPFRC), in order to emphasize the importance of steel fibers in UHPC. Even though experimental researches have proved that the use of steel fibers in UHPC have great influence on the mechanical and durability properties of its specimens and structural members, researchers are yet to model its geometry into UHPC specimens and members before they can be used in finite element numerical simulation.

Some studies on the modelling of steel fibers and assembling them into steel fiber reinforced concrete (SFRC) specimens have been reported. Xu et al. [19] reported an axisymmetric meso-scale modelling of hooked end steel fiber with ANSYS and VPG software packages to simulate Split Hopkinson Pressure Bar (SHPB) tests of SFRC cylindrical specimens. The fiber locations and orientations were assumed to be randomly distributed and a MATLAB program was used to generate them. The model yielded good results but it is only suitable for small size specimens. Liang and Wu [20] also developed a meso-scale modelling of steel fiber reinforced concrete prism with high strength based on Delaunay triangulation; and results showed that high fidelity of numerical simulations was achieved. Fang and Zhang [21] investigated three-dimensional (3D) modelling of SFRC subjected to intense dynamic loading; and reported that the model predicts the response of the SFRC specimen better than the homogeneous concrete model that is frequently used by researchers. Most of the studies on SFRC modelling were developed on the basis that the model is two dimensional (2D) or pseudo 3D. More so, the SFRC specimens were limited to small size cubes or cylinders or prisms because manual process was employed in placing the steel fibers in their locations; and this will be a very cumbersome task for large specimens (like beams, columns, and slabs) that may contain hundreds of thousands/millions of steel fibers.

There exist several reports on the numerical modelling and simulation of the properties of UHPC specimens or members, and discrepancies have been found to exist between the experimental results and the numerical results because steel fiber was not geometrically modelled and placed in the assembled member model. For example, 16% difference in both ultimate load and deflection was found between experimental and numerical (simulated using ABAQUS) results of the UHPC column in Hashim et al. [22] research on developing a constitutive and damage plasticity models for UHPFRC with different types of fiber. Also, analysis of the crack and failure pattern of the UHPC beams subjected to four-point shear loading arrangement in Bahij et al. [23] numerical investigation showed that the numerical results of the crack (especially the formation of double diagonal cracks) and failure pattern, as well as the post-peak load-midspan deflection behavior vary greatly from the experimental results. In Solhmirzaei et al. [24] investigation of the shear behavior of UHPC beams without stirrups, the numerical results of the ultimate shear capacity of all the beams were lower than the experimental results because steel fibers were not incorporated into the modelled beams. The numerical results of the ultimate shear capacity of the UHPFRC-normal strength concrete (NSC)/high strength concrete (HSC) having shear span-depth ratio of 3.0, longitudinal reinforcement ratio of 0.081 and 2% volume of steel fiber investigated by Hussein [25] was below the experimental results because steel fibers were not incorporated into the model. Despite the availability of many researches on the numerical simulation of UHPC members' properties, they have all been modelled like normal or reinforced concrete with adjustments to only material parameters based on tests results; and this approach has led to:

- Wide discrepancies (usually lower values of numerical results) between experimental results and simulation results.
- Inability to study the effect of steel fibers (i.e., steel fiber volume fraction or aspect ratio or type of steel fiber) on the UHPC member's behavior through numerical modelling and simulation, except through the casting of specimens for the different parameters to be studied, and experimentally testing their mechanical properties in order to obtain their different material properties for modelling.
- High experimental cost from the preparation of different specimens for the different steel fiber parameters, in order to obtain their material properties for modelling if the effect of steel fiber on UHPC is to be studied.

To the best knowledge of the authors, no numerical modelling of steel fibers has been reported for UHPC members' simulation, and so, no systematic way of investigating the effects of steel fiber volume fraction or aspect ratio or type of steel fiber on UHPC members' properties through numerical modelling and simulation. So, this study seeks to present a simplified way of using numerical simulation to investigate the influence of steel fibers on UHPC properties or members' behavior at the lowest possible cost and shortest time, in which the steel fibers are automatically generated and placed in their random positions without manual placement.

2 Methodology of steel fiber modelling

This steel fiber modelling technique is divided into two parts. The first part deals with the calculation of the number of steel fibers in a UHPC specimen; and the second part deals with the generation of the steel fibers' location, orientation and their assembling. The significance of this method can be seen in three innovative ways. The first is its ability to be applied to both small and big size UHPC specimens. The second innovation is seen in the ability of the python script file to be run directly in ABAQUS for the automatic generation and placement of the steel fibers in their random location based on their orientation. The third innovative nature of this method is the inclusion of the part that takes care of both wall effect and size effect in the algorithm; in order to ensure that the steel fibers close to the boundaries of the specimens are aligned near the boundary surfaces and prevented from being placed outside the specimen boundaries.

2.1 Estimation of the number of steel fibers in a UHPC specimen or member

Generally, the steel fibers used in UHPC are of circular shape; and as straight steel fibers were used for this study, the circular shape was adopted. The total volume of steel fibers (V_{tsf}) present in a given volume of UHPC specimen (V_{sp}) wholly depends on the percentage of steel fiber volume fraction (V_f expressed in percentage) and the dimension of the specimen [26]. So, it can be estimated using Eq. (1).

$$V_{tsf} = \frac{V_{sp}V_f}{100} \tag{1}$$

The volume of a single steel fiber (V_{ssf}) depends on its diameter (d) and length (L); and so, it is expressed as the products of its area (A_{sf}) and length as in Eq. (2).

$$V_{ssf} = A_{sf}L = \frac{\pi d^2 L}{4}, \tag{2}$$

where π is a constant called pie = 22/7

Therefore, the number of steel fibers (n_{sf}) in any UHPC specimen can be estimated as:

$$n_{sf} = \frac{V_{tsf}}{V_{ssf}}. \tag{3}$$

2.2 Generation of random steel fibers' location and orientation in a UHPC specimen or member

An algorithm developed using Python programming language for generating random fibers in a given area was used to generate the location and orientation of the steel fibers. The advantage of using Python code according to Blueberry Blackcurrant [27] is that, the script can be run directly in ABAQUS to generate any number of steel fibers and place them in their required location based on their orientation; thereby saving the time and energy that will be spent in placing large number of steel fibers in a UHPC member. This algorithm also builds the UHPC specimen alongside the steel fibers. The algorithm has four different parts:

- The first part is the "def intersection" part that takes care of practical placement requirements of fibers in UHPC members by checking the spatial relationship between the generated numbers of fibers, in order to prevent their intersection.
- The second part is the "def fiber location" part. This part is divided into three sub-parts. The first sub-part is where concrete member is represented in the algorithm as a rectangular specimen with length (L), height (H) and breadth (B). The second sub-part is where steel fiber is represented with fiber length

and fiber number evaluated using Eq. (3). The third sub-part is the part where the orientation of the fiber which by default rotates freely within 360° was introduced as an evenly distributed random variable with one of its end point determined and recorded as ipoint (i.e., the starting point). Then with ipoint known, the fiber length is rotated within 360° to determine epoint (i.e., the second end point).

- The third part is the "Building the concrete part" where the concrete geometry is generated.
- The fourth part is the "Combination Assembly" part where both the generated steel fibers and the concrete are combined as an assembled model.

The "def fiber location" part of the algorithm takes care of the wall effect and size effect by considering the concrete specimen's dimensions as well as the initial and end points of the steel fiber. These effects were built as fiber-specimen wall intersection signal in the algorithm. If the signal is confirmed to be true, it takes the fiber position as $i + 1$ instead of i. If the signal is false, the fiber position is taken as i. With this part of the algorithm, the steel fibers are prevented from being placed outside the specimen's boundary and automatically programmed from making contact with the walls of the concrete specimen. The algorithm needs to be copied from Python software to Notepad and saved. After which ABAQUS is opened and the script run (submenu) in the file menu (around the upper left corner) of ABAQUS is clicked. And then the saved Notepad file is selected for the geometry of the UHPC specimen or member and steel fibers to be automatically generated. The algorithm for UHPC beam of 1000 mm length, 100 mm height and 50 mm breadth containing 1% volume of steel fiber of 40 mm length and 0.9 mm diameter is as follows:

```
# coding=UTF-8
fromabaqusConstantsimport*
fromcaeModulesimport*
importnumpyasnp
importmath

defintersection (a,b):
    a1 =list(a[0])
    a2 =list(a[1])
    b1 =list(b[0])
    b2 =list(b[1])

    v1 =np.cross(np.array(a1) -np.array(b1), np.ar-
    ray(b2) -np.array(b1))
    v2 =np.cross(np.array(a2) -np.array(b1), np.ar-
    ray(b2) -np.array(b1))
    dot_value= np.dot(v1, v2)/(np.linalg.norm(v1)
    *np.linalg.norm(v2))
    v11 =np.cross(np.array(b1) -np.array(a1), np.ar-
    ray(a2) -np.array(a1))
    v21 =np.cross(np.array(b2) -np.array(a1), np.ar-
    ray(a2) -np.array(a1))
    dot_value1 = np.dot(v11, v21)/(np.linalg.
    norm(v11) *np.linalg.norm(v21))

    if dot_value==-1and dot_value1 ==-1:
        return1
    else:
        return0

deffiberlocation (b):
    Psi =np.random.uniform(0,2*math.pi)
    Theta =np.random.uniform(0,2*math.pi)
    x = b[0] +fiberlength*math.sin(Psi) *math.
    sin(Theta)
    y = b[1] +fiberlength*math.sin(Psi) *math.
    cos(Theta)
    z = b[2] +fiberlength*math.cos(Psi)
    endpoint = (x,y,z)
    return endpoint

#Enter the length, height, and width of the delivery area, the
number of fibers in the delivery area and the value of the fiber
length (the 5 parameters are selected according to your own
needs)

L =1000.0
H =100.0
B =50.0
fiberlength=40
fibernumber=1965

fiber= [] *fibernumber
initialfiber= (np.random.uniform(-(H/2-fiberlength),
    (H/2-fiberlength)),np.random.uniform(-(B/2-fi-
    berlength),(B/2-fiberlength)),np.random.
    uniform(-(L/2-fiberlength),(L/2-fiberlength)))
fiber.append((initialfiber,fiberlocation(initial-
    fiber)))

i =1
while i <fibernumber:
    ipoint= (np.random.uniform(-H/2,H/2),np.random.
    uniform(-B/2,B/2),np.random.uniform(-L/2,L/2))
    epoint=fiberlocation(ipoint)
    if abs(epoint[0])<H/2 and abs(epoint[1])<B/2 and
    abs(epoint[2])<L/2:
        for j inrange(0, i):
            signal = intersection(fiber[j],
    (ipoint, epoint))
            if signal isTrue:
                break
        fiber.append((ipoint, epoint))
        i = i +1
    else:
        continue
```

```
myModel=mdb.Model(name='Model-1')
p =myModel.Part(name='fiber',
    dimensionality=THREE_D,
    type=DEFORMABLE_BODY)
    p.ReferencePoint(point=(0.0, 0.0, 0.0))

for j inrange (0,fibernumber):
    p.WirePolyLine(points=(fiber[j][0], fiber[j]
    [1]), mergeType=IMPRINT, meshable=ON)

delp.features['RP']

#Building the concrete part

s =mdb.models['Model-1'].
    ConstrainedSketch(name='__profile__',
    sheetSize=200.0)
g, v, d, c =s.geometry, s.vertices, s.dimensions,
    s.constraints
s.setPrimaryObject(option=STANDALONE)
s.Line(point1=(-H/2, -B/2), point2=(-H/2, B/2))
s.VerticalConstraint(entity=g[2],
    addUndoState=False)
s.Line(point1=(-H/2, B/2), point2=(H/2, B/2))
s.HorizontalConstraint(entity=g[3],
    addUndoState=False)
s.PerpendicularConstraint(entity1=g[2], enti-
    ty2=g[3], addUndoState=False)
s.Line(point1=(H/2, B/2), point2=(H/2, -B/2))
s.VerticalConstraint(entity=g[4],
    addUndoState=False)
s.PerpendicularConstraint(entity1=g[3], enti-
    ty2=g[4], addUndoState=False)
s.Line(point1=(H/2, -B/2), point2=(-H/2, -B/2))
s.HorizontalConstraint(entity=g[5],
    addUndoState=False)
s.PerpendicularConstraint(entity1=g[4], enti-
    ty2=g[5], addUndoState=False)
p =mdb.models['Model-1'].Part(name='Concrete',
    dimensionality=THREE_D, type=DEFORMABLE_BODY)
p =mdb.models['Model-1'].parts['Concrete']
p.BaseSolidExtrude(sketch=s, depth=L)
s.unsetPrimaryObject()
session.viewports['Viewport: 1'].
    setValues(displayedObject=p)
delmdb.models['Model-1'].sketches['__profile__']

# Combination Assembly

a =mdb.models['Model-1'].rootAssembly
a.DatumCsysByDefault(CARTESIAN)
p =mdb.models['Model-1'].parts['Concrete']
a.Instance(name='Concrete-1', part=p,
    dependent=ON)
a.translate(instanceList=('Concrete-1', ), vec-
    tor=(0.0, 0.0, -L/2))
p =mdb.models['Model-1'].parts['fiber']
a.Instance(name='fiber-1', part=p, dependent=ON)
```

A flow chart to the algorithm is presented in Fig. 2(a) to help understand how it is used. The geometry of the UHPC beam together with the generated steel fibers, which took only six (6) minutes and twenty (20) seconds to execute using this simplified approach, is shown in Fig. 2(b).

3 Illustrative examples

These illustrative examples were carried out in order to check the correctness and accuracy of the proposed method. This is because the validity of the proposed method can only be assessed through the difference in its results and the results from experiments (which is the true and practical representation of the specimens' behavior). Also, prior to the development of this simplified method, ultra-high performance concrete specimens have always been modelled by researchers like normal concrete without including the presence of steel fibers. So, these illustrative examples

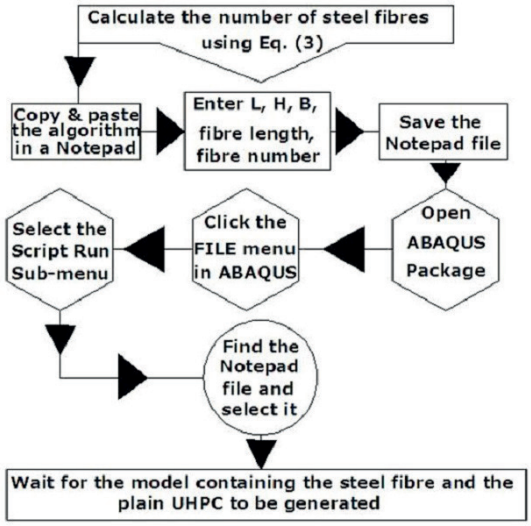

(a)

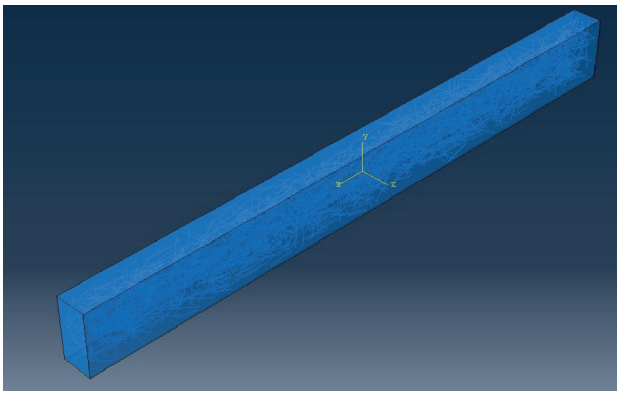

(b)

Fig. 2 (a) Flow chart to the algorithm, (b) Geometry of the UHPC beam and the generated steel fibers (Scale is 1:20 mm)

were considered through: (1) this proposed method (2) experiment (3) normal concrete modelling method without including the presence of steel fibers. And results were collected from the three different methods to see which of the results (between the proposed method and the normal concrete modelling method) is the closest to the results obtained from experiments (experimental results were taken as the reference results). If the results from the proposed method are closer to that from experiments than the results from normal concrete modelling method, then the proposed method will be considered as more effective and more accurate than the normal concrete modelling method. Otherwise, the proposed method will be considered as less effective and less accurate than the normal concrete modelling method.

3.1 Experimentation

The use of this simplified and cost-effective approach is demonstrated through two tests:

(1) The investigation of the effect of steel fiber on the compressive properties of UHPC cube specimen of 100 mm length, 100 mm height and 100 mm breadth: Three UHPC cube specimens were cast and subjected to uniaxial compression test as shown in Fig. 3 based on [28] to study its compressive properties at 2% volume of steel fibers after 28 days curing in water. Before carrying out the compressive strength test, the cubes were weighed for the evaluation of their densities and the average was taken as the density of UHPC cube specimen. The results of the compressive strength test from this experiment were compared with that obtained from numerical simulation using 0, 1 and 2% volume of steel fibers.

(2) The shear performance of ultra-high performance concrete beam: Beam specimen of size 100 × 200 × 1200 mm^3 was made in accordance with [29, 30] design principles with a clear concrete cover of 20 mm. The longitudinal reinforcement ratio (ρ) was kept at 0.0185; and the tensile reinforcement was bent up at 90° to a length of 150 mm (i.e., >3 × longitudinal tension steel diameter) and together with the compressive reinforcements was tied to the stirrups with steel wire mesh. The beam was over reinforced in flexure with 2Φ14 high strength steels in the tensile zone; 2Φ6.5 in the compression zone and 6Φ6.5 in shear to ensure only shear failure by making sure that the flexural moment of the beams exceed the moment caused by the applied shear load. For shear reinforcement, Narayanan and Darwish [14] analytical equation for steel fiber reinforced concrete design, expressed in Eq. (4) was used to design the UHPC beam.

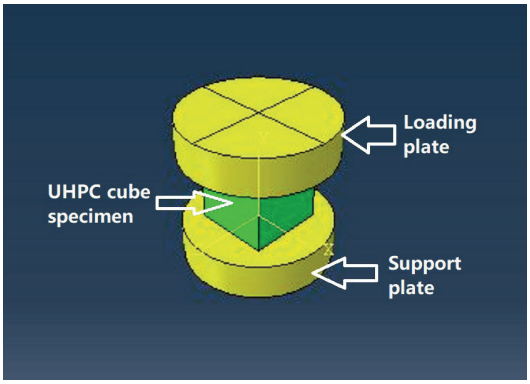

Fig. 3 Compressive strength test setup

$$V_u = V_c + V_s \tag{4}$$

$$V_c = \left[e \times \left(0.24 \left(\frac{f_c}{20 - \sqrt{F_f}} + 0.7 + \sqrt{F_f} \right) + 80\rho \frac{d}{a} \right) + 1.7F_f \right] bh \tag{5}$$

$$F_f = \frac{l_f}{d_f} \times V_f \times \alpha \tag{6}$$

$$V_s = \frac{A_{ss} f_{ys} d}{s}; M_{Vu} = \frac{2 \times V_u}{a} \tag{7}$$

$$M_f = A_{sl} f_{yl} \left(d - \frac{a_e}{2} \right) + \sigma_p b (h - c) \left(\frac{h + c - a_e}{2} \right) \tag{8}$$

$$\sigma_p = 0.85 V_f \tau_f \frac{l_f}{d_f}; a_e = \frac{A_{sl} f_{yl} + \sigma_p bh}{\eta f_c b + \sigma_p b}; c = \frac{a_e}{\beta_1} \tag{9}$$

Where, V_u is ultimate shear force; V_c is shear force in UHPC; V_s is shear force in stirrups; e is arch action factor = 1.0 for $a/d > 2.5$ and 2.5 d/a for $a/d < 2.5$; f_c is compressive strength of UHPC; F_f is fiber factor; l_f is length of fiber; d_f is diameter of fiber; V_f is fibre volume fraction; α is bond factor = 0.5 for straight steel fiber; ρ is longitudinal reinforcement ratio; d = effective depth of the beam; a is shear span; b is breadth of the beam; h is the height of the beam; A_{ss} is cross sectional area of two-legged stirrups; f_{ys} is yield stress of stirrup; s is stirrup spacing; M_{Vu} is moment due to applied shear load; M_f is flexural moment of the beam; A_{sl} = cross sectional area of longitudinal reinforcement; a_e is depth of equivalent compressive block of beam; σ_p is post cracking strength of fiber reinforced composite; c is neutral axis depth of beam; τ_f is frictional bond strength of fiber matrix = $0.66\sqrt{f_c}$ in N/mm^2; f_{yl} is yield stress of longitudinal reinforcement; η is concrete stress block parameter = 0.86 for $f_c \geq 55$ N/mm^2; and β_1 is concrete stress block parameter = 0.65 for $f_c \geq 55$ N/mm^2.

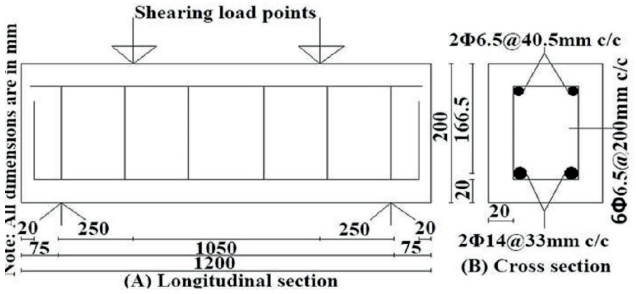

Fig. 4 Longitudinal-cross sections of the UHPC beam with stirrups

Fig. 4 shows the longitudinal-cross section of the UHPC beam under shear load application.

Two UHPC beam specimens, one with stirrups and one without stirrups were cast for shear test. The beam with stirrups was designed to have 200 mm c/c stirrup spacing and the two beams were subjected to four-point loading configuration using shear span-effective depth ratio (a/d) of 1.5. Load and displacement control system was used to apply the shear load in order to determine the UHPC beams' cracking strength, ultimate strength, midspan deflection, crack pattern and failure mode in accordance with GB/T 50152 [31]. The cracking strength and ultimate strength were measured from the load cell on the hydraulic jack, while the crack pattern and failure mode were observed and analyzed. Two strain gauges were glued and soldered to two stirrups, one each on the stirrup after each support to measure the strains in the stirrups. Also, three strain gauges were fixed on the UHPC beams to measure its strains in accordance with GB/T 50152 [31] procedure. And three dial gauges were mounted on the beam, one at the concrete midspan and the remaining two at the two supports (that is 75 mm from the two ends of the beam) to measure the midspan displacement of the beam at every loading step as illustrated in Fig. 5.

Modified Andreasen and Andersen model [32] expressed in Eq. (10) was employed for the UHPC mixture design; and the mixture proportion for 1 m^3 UHPC specimen is shown in Table 1.

$$P(D) = 100 \times \frac{D^q - D_{\min}^q}{D_{\max}^q - D_{\min}^q}, \tag{10}$$

where, $P(D)$ is the volume fraction of the total solids smaller than size D; D is the particle size (μm); D_{max} is the maximum particle size (μm); D_{min} is the minimum particle size (μm); q is the distribution modulus ($q < 0.25$ for fine particles).

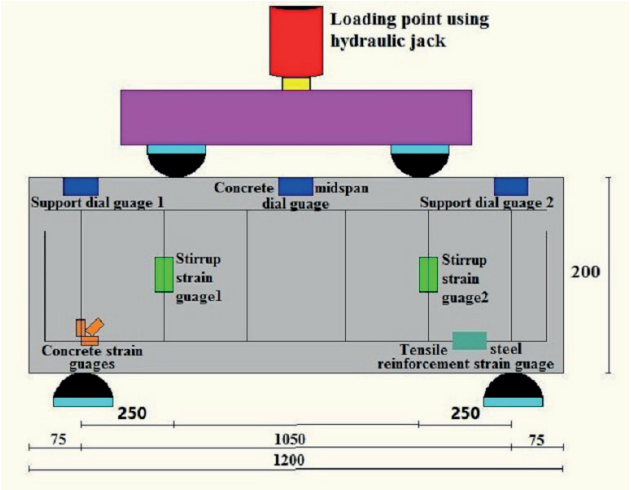

Fig. 5 Shear test set up

Table 1 Mix proportion for 1 m^3 UHPC beam

UHPC ingredients	Quantity (kg/m^3)
P.O 52.5 Cement	461.01
P.C 42.5 Cement	322.70
Quartz sand (≤1 mm)	922.01
Granite (5–10 mm)	412.50
Silica fume	138.30
Steel fibers	133.45
Superplasticizer	22.50
Water	166.25

3.2 Material and geometry modelling

The cube and beam models (geometry, materials, and constraints) were both developed using ABAQUS/CAE 2017 software and finite element analysis method was used to simulate the shear performance of the UHPC beam. In terms of geometry, the steel fibers through the algorithm in Section 2.2 was modelled as three-dimensional (3D), hex-deformable wire beam element; while the UHPC, also through the same algorithm was modelled using the three-dimensional (3D), hex-deformable solid (brick) element having three degrees of freedom at each of its nodes. The stirrup in the beam was modelled using the three dimensional (3D), hex-deformable wire truss element. The steel-plates used for supports and load points, and steel reinforcements were modelled using the three-dimensional (3D), hex-deformable solid (brick) elements having three degrees of freedom at each of its nodes. Fig. 6(a) shows the generated 1% volume of steel fiber (containing 24485 steel fibers) in the UHPC cube and Fig. 6(b) shows the generated 2% volume of steel fiber (containing 1175298 steel fibers) in the UHPC beam.

Material wise, the steel fiber, tensile and compressive steel reinforcements, stirrups, support and load plate were modelled using elastic-plastic approach using its properties (provided by the manufacturer) shown in Table 2. These parameters among many others are default parameters

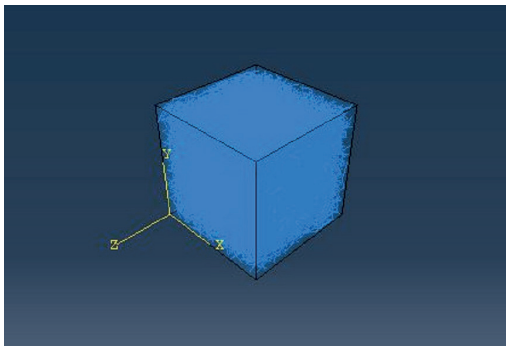

(a)

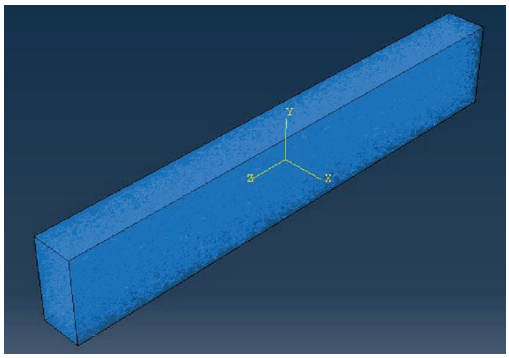

(b)

Fig. 6 (a) Generated 1% volume of steel fiber in UHPC cube (Scale is 1:10 mm), (b) Generated 2% volume of steel fiber in UHPC beam (Scale is 1:20 mm)

Table 2 Material modelling parameters

Parameter	UHPC	Steel reinforcement		Steel fiber
		14 mm	6.5 mm	
Compressive strength (N/mm^2)	157	-	-	-
Tensile strength (N/mm^2)	6.52	702	552	-
Yield stress(N/mm^2)	-	650	414	2850
Elastic modulus (N/mm^2)	44600	210000	210000	210000
Poisson's ratio	0.2	0.3	0.3	0.3
Density (kg/mm^3)	2.5E-9	7.8E-9	7.8E-9	7.8E-9
Dilation angle ψ (o)	33	-	-	-
Eccentricity	0.1	-	-	-
$fb0/fc0$	1.16	-	-	-
K	0.667	-	-	-
Viscosity parameter	0	-	-	-
Diameter (mm)	-	-	-	0.20
Length (mm)	-	-	-	13

programmed in ABAQUS package for the material modelling of structural specimens or members. The choice of parameters for the numerical simulation of any structural element in ABAQUS therefore depends on the type of Finite Element Analysis (FEA); and since dynamic explicit analysis was employed for this study, the parameters in Table 2 were automatically chosen by default.

Plastic-damage model for concrete developed by Lubliner et al. [33], which states that plastic degradation occurs only in the softening range and that the stiffness is proportional to the cohesion of the material as shown in Eq. (11), was employed as it is the only ABAQUS model with the capability of not only studying the inelastic behavior of UHPC but can also be used to perform UHPC's static and dynamic analysis.

$$\frac{E}{E_0} = \frac{c}{c_{\max}} = 1 - d \,, \tag{11}$$

where c and $c_{\max}$ are the cohesion in the yield criteria which is proportional to stress and the strength of the concrete respectively; E and E_0 are the current degraded stiffness and initial (that is undamaged) elastic stiffness respectively; and d is the plastic degradation.

So, the UHPC was modelled with elastic and concrete damage plasticity (CDP) concept using the mechanical properties determined from uniaxial compressive strength, tensile strength, elastic modulus and Poisson's ratio experiments and other required parameters shown in Table 2. Besides the three UHPC cubes tested for uniaxial compressive strength, three UHPC dog-bone specimens were cast, cured for 28 days and tested for tensile strength in accordance with T/CBMF37-2018 [34] recommendation. Also, three prismatic specimens were cast using 100 mm × 100 mm × 300 mm mold and cured for 28 days to determine the elastic modulus and Poisson's ratio of the UHPC specimens in accordance with CECS13-2009 [35] specification. The default values in ABAQUS for dilation angle ψ(°), eccentricity, ratio of initial equibiaxial compressive yield stress to the initial uniaxial compressive yield stress ($fb0/fc0$), ratio of the second stress invariant on the tensile meridian to that on the compressive meridian (K), and viscosity parameter were used for this study. Concrete damage plasticity (CDP) approach described in Eq. (12), develops the constitutive behavior of the UHPC cubes and beams by presenting the scalar damage variables for both compressive and tensile response (i.e., damage variable in tension, d_t and damage variable in compression, d_c) under uniaxial loading.

$$\sigma = (1-d)E_o\left(\varepsilon - \varepsilon^{pl}\right), \tag{12}$$

where σ is the stress; ε is the total strain and ε^{pl} is the plastic strain.

The CDP approach describes mainly two failure mechanisms: tensile cracking and compressive crushing of concrete. The yield surface is governed by two hardening variables: plastic strain corresponding to tensile strength of concrete (ε_t^{pl}) and plastic strain corresponding to compressive strength of concrete (ε_c^{pl}), which are associated to the failure mechanisms under tension and compression loading respectively. The compressive and tensile damage needed to model the non-linear and complex behavior of concrete in ABAQUS were estimated through Eqs. (13) and (14) [36] using the experimental data in Table 2 and Fig. 7 (stress-plastic strain values).

$$d_c = 1 - \frac{\sigma_c E_c^{-1}}{\varepsilon_c^{pl}\left(\frac{1}{b_c}-1\right)+\sigma_c E_c^{-1}} \quad or$$

$$d_c = 1 - \frac{\sigma_c E_c^{-1}}{\varepsilon_c^{in}\left(1-b_c\right)+\sigma_c E_c^{-1}} \tag{13}$$

$$d_t = 1 - \frac{\sigma_t E_t^{-1}}{\varepsilon_t^{pl}\left(\frac{1}{b_t}-1\right)+\sigma_t E_c^{-1}} \quad or$$

$$d_t = 1 - \frac{\sigma_t E_t^{-1}}{\varepsilon_t^{in}\left(1-b_t\right)+\sigma_t E_c^{-1}} \tag{14}$$

$$\varepsilon_c^{pl} = \varepsilon_c^{in} - \frac{d_c\sigma_c}{(1-d_c)E_o} \tag{15}$$

$$\varepsilon_t^{pl} = \varepsilon_t^{cr} - \frac{d_t\sigma_t}{(1-d_t)E_o} \tag{16}$$

$$\varepsilon_c^{in} = \varepsilon_c - \varepsilon_c^{el} \quad or \quad \varepsilon_c - \frac{\sigma_c}{E_o} \tag{17}$$

$$\varepsilon_t^{cr} = \varepsilon_t - \varepsilon_t^{el} \quad or \quad \varepsilon_t - \frac{\sigma_t}{E_o} \tag{18}$$

Where d_c, d_t, σ_c, σ_t, E_o, ε_c, ε_t, ε_c^{pl}, ε_t^{pl}, ε_c^{el}, ε_t^{el}, ε_c^{in} and ε_t^{cr} are compressive damage parameter which ranges from 0 to 1, tensile damage parameter which ranges from 0 to 1, compressive stress of concrete, tensile stress of concrete, modulus of elasticity of concrete, total concrete strain in compression, total concrete strain in tension, plastic strain corresponding to compressive strength of concrete, plastic strain corresponding to tensile strength of concrete, elastic strain of concrete in compression, elastic strain of concrete in tension, inelastic strain of concrete in compression, cracking strain of concrete in tension respectively. b_c and b_t are constant parameters with values $0 < b_c, b_t \leq 1$ ($b_c = 0.7$ and $b_t = 0.1$).

Considering the constraints and interaction applied to the UHPC cube, firstly, the steel fibers in the UHPC was modelled as steel fibers in embedded region with the plain UHPC acting as the host region and the steel fibers acting as the embedded element. Secondly, the support and load point surfaces of the UHPC cube were modelled using rigid body tie constraint. Thirdly, the support point of the plain UHPC was modelled using fixed support boundary condition; and a displacement load was applied at the loading point of the UHPC cube using dynamic explicit procedure to carry out Finite element numerical simulation of the uniaxial compression of the UHPC cube at 0, 1 and 2% volume of steel fiber. In terms of the constraints and interaction applied to the UHPC beams, tie constraint

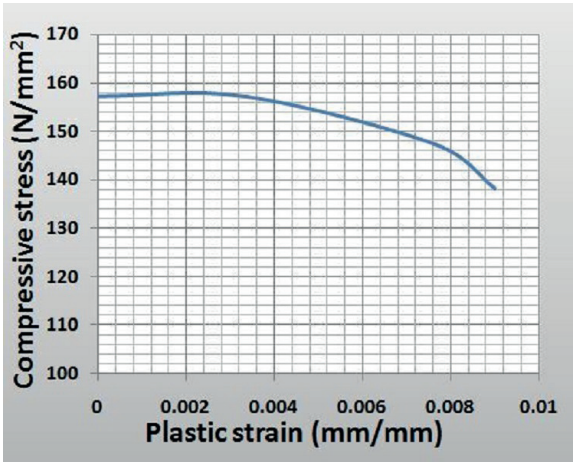

(a)

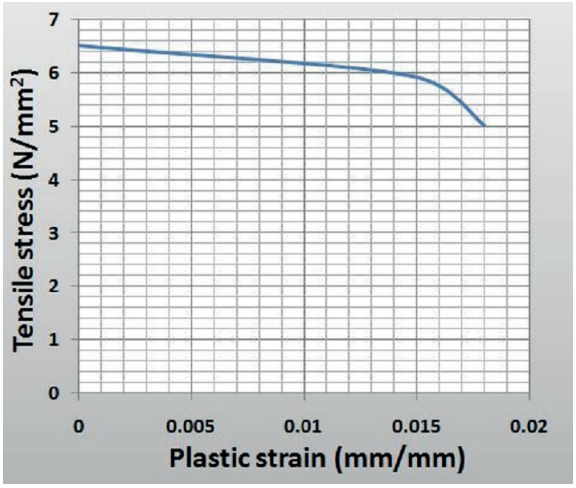

(b)

Fig. 7 (a)Compressive stress-plastic strain curve, (b) Tensile stress-plastic strain curve

was applied to model the surface of the UHPC beam to the surfaces of the supports and load points, with the plain UHPC acting as the slave surface; and the supports and load point surfaces acting as the master surfaces. Also, the steel fiber, tensile and compressive steel reinforcements and stirrups were modelled as steel fiber-tensile and compressive steel reinforcements-stirrups in embedded region, with the plain UHPC acting as the host region and the steel fiber-tensile and compressive steel reinforcements-stirrups acting as the embedded element. Pinned support boundary condition was used to model the supports of the beams; while displacement load was applied at the load points using dynamic explicit procedure with a time period of two seconds to carry out the numerical finite element analysis of the shear performance of the UHPC beams.

The assembled UHPC cube containing the plain UHPC cube and steel fibers were seeded using the mesh size of 10 mm; while the assembled beam containing plain UHPC, steel reinforcement, supports and load point plates was seeded using the same mesh size of 20 mm to avoid the problem of node incompatibility. Fig. 8(a) and Fig. 8(b) illustrate the geometry (containing the constraints and boundary conditions) and the meshed UHPC cube, respectively, while Fig. 8(c) and Fig. 8(d) show the geometry and the meshed UHPC beam.

4 Results and discussions

4.1 Failure mode and deformation pattern of the UHPC cube

The UHPC cube for 0, 1 and 2% volume of steel fiber all have type 6 failure modes according to [37]. Fig. 9(a) shows that the cube with 0% volume of steel fiber has a highly dense deformation pattern that is more concentrated at the right-hand side of the cube than the left-hand side. The deformation pattern of the cube with 1% volume of steel fiber as shown in Fig. 9(b) is similar to that with 0% volume of steel fiber except that it has a less dense deformation and projects more towards the center than that of 0% volume of steel fiber. The deformation pattern of the cube with 2% volume of steel fiber is less dense than that with 1% volume of steel fiber as can be seen in Fig. 9(c). The difference between the three UHPC cube containing 0, 1 and 2% volume of steel fibers is in the density of their deformation in terms of cracks represented by red coloration in Fig. 9(a)–(c). While Fig. 9(a) has the most deformation, Fig. 9(b) underwent lesser deformation than Fig. 9(a) and Fig. 9(c) has the least deformation. This means that as the % volume of steel fiber increases in a UHPC cube, the cube will undergo less deformation before its failure. The ability of the cube to undergo less deformation when steel fiber is added to the cube mix may be due to the ability of the steel fibers to bear the stress on the cube and re-distribute them

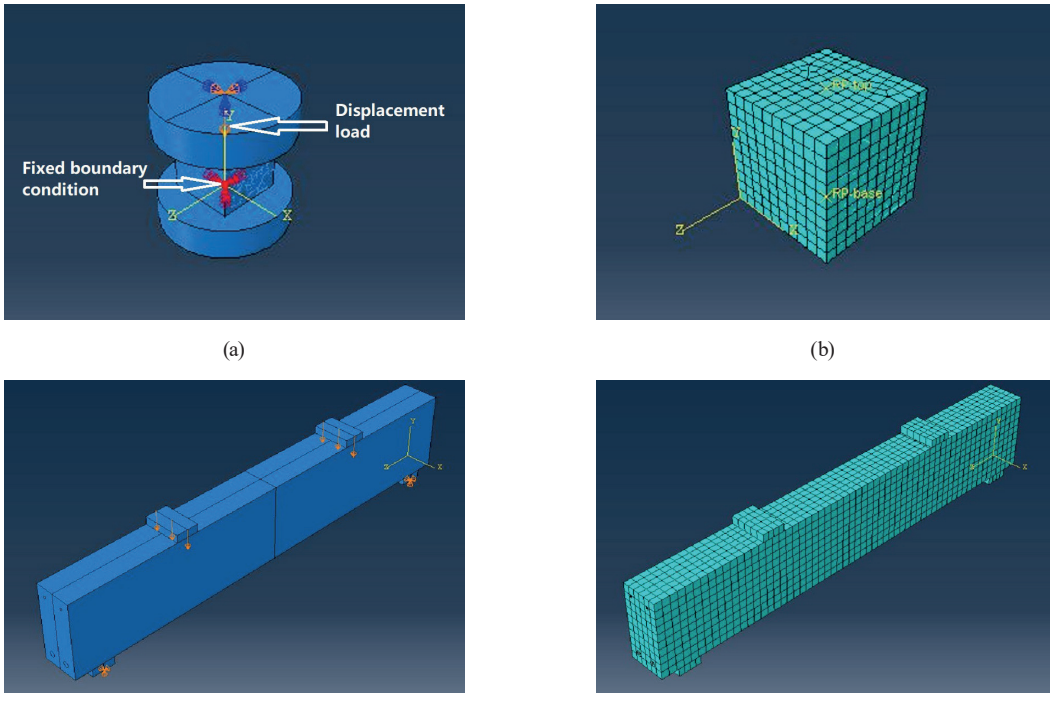

Fig. 8 (a) UHPC cube geometry and boundary condition, (b) Meshed UHPC cube (Scale is 1:10 mm), (c) UHPC beam geometry and boundary condition (Scale is 1:20 mm), (d) Meshed UHPC beam (Scale is 1:20 mm)

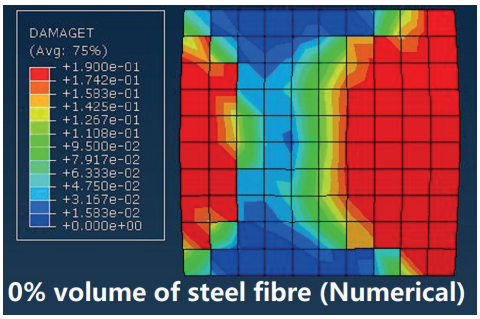

(a)

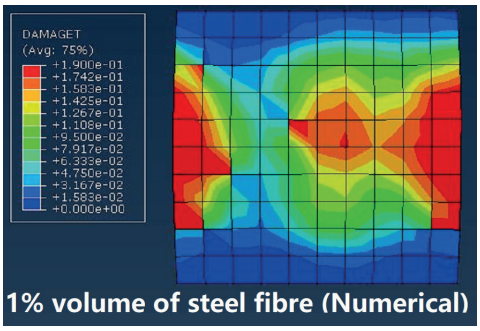

(b)

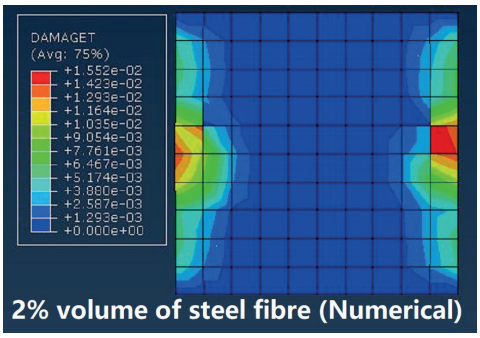

(c)

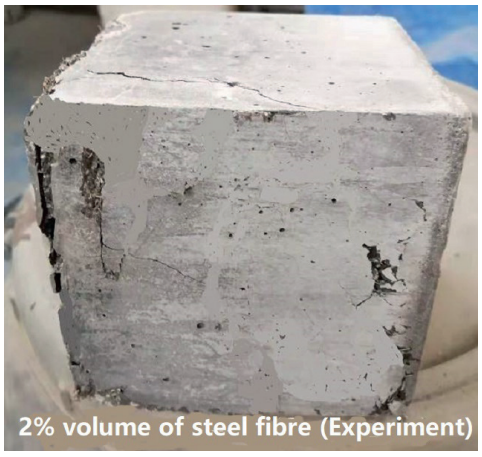

(d)

Fig. 9 (a) Deformation pattern of UHPC cube with 0% volume of steel fiber (Numerical), (b) Deformation pattern of UHPC cube with 1% volume of steel fiber (Numerical), (c) Deformation pattern of UHPC cube with 2% volume of steel fiber (Numerical), (d) Deformation pattern of UHPC cube with 2% volume of steel fiber (Experiment)

to other parts of the cube [38]; and the reason for less deformation when the cube' steel fiber volume is increased is due to the stress been borne by more steel fibers. Furthermore, Fig. 9(d) shows that for 2% volume of steel fiber, the failure mode and deformation pattern of the UHPC cube from experiment is in total agreement with that from numerical simulation. Also, the deformation pattern of the cube with 0% volume of steel fiber is completely different from the two cubes with 1 and 2% volume of steel fibers, even though the material properties of the UHPC cube with 2% volume of steel fiber obtained from experiment was used to model it. This clearly shows that this approach of readjusting the material properties (that has been employed by researchers) in modelling steel fiber reinforced concrete or ultra-high performance concrete specimens and members for simulation cannot give reliable results; and so, this simplified approach can be used to get a more reliable results of the true failure mode and deformation pattern of UHPC cube specimens.

4.2 Compression force-displacement behavior of the UHPC cube

Fig. 10 illustrates the compression force-displacement relationship of the UHPC cube and the results displayed similar trend for both experiment and numerical simulation (for the cubes modelled with steel fiber). The results showed that increase in % volume of steel fibers in the UHPC cube leads to increase in compressive force and decrease in deformation (in terms of displacement) of the cube. So, if a UHPC cube specimen is modelled and numerically simulated for compressive strength without including the physical geometry of steel fibers (as it is being done by researchers), as represented in this study by 0% volume

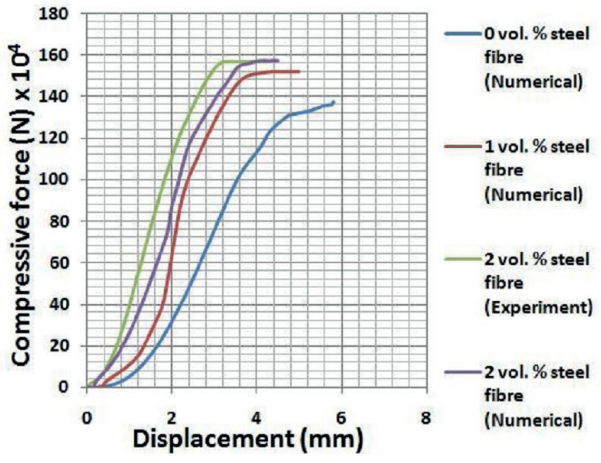

Fig. 10 Uniaxial compressive force-displacement curve of the UHPC cube

of steel fiber, the ultimate simulated values of compression force and displacement will be much different from the experimental values. The experimental cube (containing 2% volume of steel fibers) has an ultimate compressive force and displacement of 1570000 N and 4.25 mm, respectively, while the numerically simulated cube (containing 2% volume of steel fibers) has an ultimate compressive force and displacement of 1575000 N and 4.5 mm respectively. However, the numerically simulated cube containing 0% volume of steel fiber has an ultimate compressive force and displacement of 1380000 N and 5.80 mm, respectively. Further analysis revealed that the ultimate compressive force of the numerically simulated cube containing 2% volume of steel fibers is only 0.3% higher than the experimental cube containing 2% volume of steel fibers; while the ultimate compressive force of the numerically simulated cube containing 0% volume of steel fibers (which is always used by researchers to represent the numerical model of UHPC cube specimen) is about 12.1% lower than the experimental cube containing 2% volume of steel fibers. This means that the inclusion of the 2% volume of steel fiber in the numerical model of the UHPC cube contributed about 12.4% additional resistance to the compression force on the UHPC cube. Also, the outcome of both the experimental and numerically simulated cubes containing 2% volume of steel fibers showed that the cubes exhibit a ductile behavior; and this may be due to the presence of steel fibers that continued to bear the compression force applied on the UHPC cube even though it has attained its ultimate compression strength. So, the numerically modelled UHPC cube specimen containing the same % volume of steel fibers as that of the experiment has better correlation with the experimental cube than the numerically modelled cube without steel fibers.

4.3 Failure mode and crack pattern of the UHPC beams

The UHPC beam with stirrups as can be seen in Figs. 11(a)–(c) for both experiment and numerical simulation failed in shear compression with two diagonal cracks within the shear zones. The first crack in the beam was a flexural crack and appeared at a load value of 35 kN for the experimental beam, 39 kN for the numerically simulated beam with stirrups and steel fibers, and 30 kN for the numerically simulated beam with stirrups but without steel fibers. The first shear crack was noticed at 76 kN for the experimental beam, 80 kN for the numerically simulated beam with stirrups and steel fibers, and 67 kN for the numerically simulated beam with stirrups but without steel fibers.

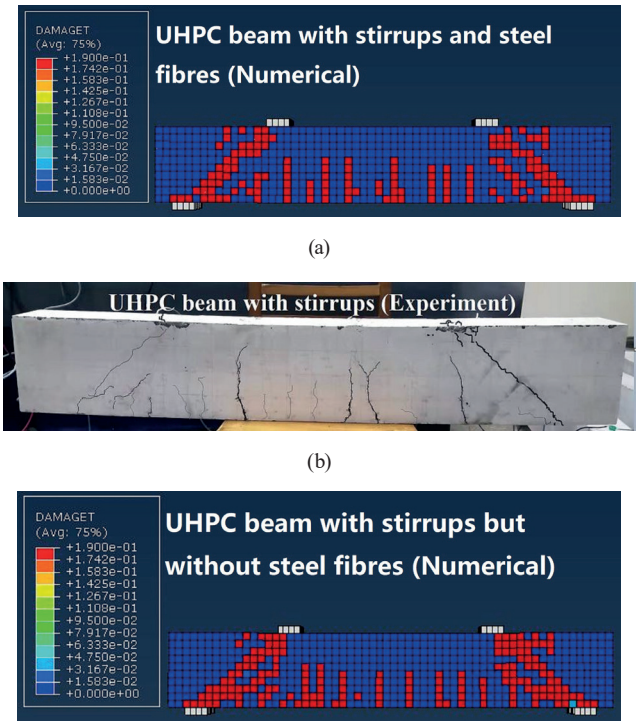

Fig. 11 (a) Crack pattern of UHPC beam with stirrups and steel fibers (Numerical), (b) Crack pattern of UHPC beam with stirrups (Experiment), (c) Crack pattern of UHPC beam with stirrups but without steel fibers (Numerical)

As the applied load was continuously increased beyond the cracking load, more cracks developed in the UHPC beam and the length and width of existing cracks slowly increased until it attained its ultimate load where the crack length and width greatly increased. This behavior of slow growth in crack length and width, which is the same for the experimental beam and the numerically simulated beam with stirrups and steel fibers, may be as a result of the ability of the UHPC to re-distribute stress to other parts of the beam because of steel fibers in its mix [38]. Through this simplified and cost-effective method of modelling the geometry of steel fibers in the UHPC beam, the contribution of steel fibers to the resistance of the numerically simulated beam at the face of shear crack appearance was easily evaluated, and the result showed that the physical presence of steel fibers improved the beam's resistance by 16.25% at the appearance of the first shear crack. Also, the crack pattern in Fig. 11 shows that the crack pattern of the UHPC beam modelled with stirrups and steel fibers (Fig. 11(a)) is similar to that of the experimental beam (Fig. 11(b)), unlike the beam modelled with stirrups but without steel fibers shown in Fig. 11(c) (which is the usual way of modelling UHPC beam for numerical simulation

by researchers) which underwent higher deformation in terms of enlarged shear cracks. This clearly reveals the importance of including steel fibers in UHPC models.

The mode of failure of the UHPC beam without stirrups as shown in Fig 12(a)–(c) for both experiment and numerical simulation was diagonal tension failure with the initial formation of flexural cracks that increased in width and length, and later developed into diagonal shear cracks. This failure mode may be as a result of the absence of shear reinforcement which led to reduction of stiffness of the UHPC beam after reaching its peak force. The beam has a cracking load of 33.5 kN for the experimental beam, 36 kN for the numerically simulated beam without stirrups but with steel fibers, and 28.5 kN for the numerically simulated beam without both stirrups and steel fibers. As the load increased, shear crack appeared at a load of 72 kN for the experimental beam, 75 kN for the numerically simulated beam without stirrups but with steel fibers, and 64.5 kN for the numerically simulated beam without both stirrups and steel fibers. Further analysis revealed that the inclusion of steel fiber in the modelled UHPC beam improved the beam's shear resistance by 14% at shear cracking face; and the absence of stirrups in the beam reduced the beam's resistance at the development of the first shear crack by 5.3 and 6.3% for the experimental beam and the numerically simulated beam without stirrups but with steel fibers respectively. On comparing the beams' crack pattern, it can be obviously seen that the crack pattern of the numerically simulated beam without stirrups but with steel fibers (Fig. 12(a)) agrees perfectly with that of the experiment (Fig. 12(b)); while the numerically simulated beam without both stirrups and steel fibers (Fig. 12(c)) has too large shear cracks that disagree with that of the experiment.

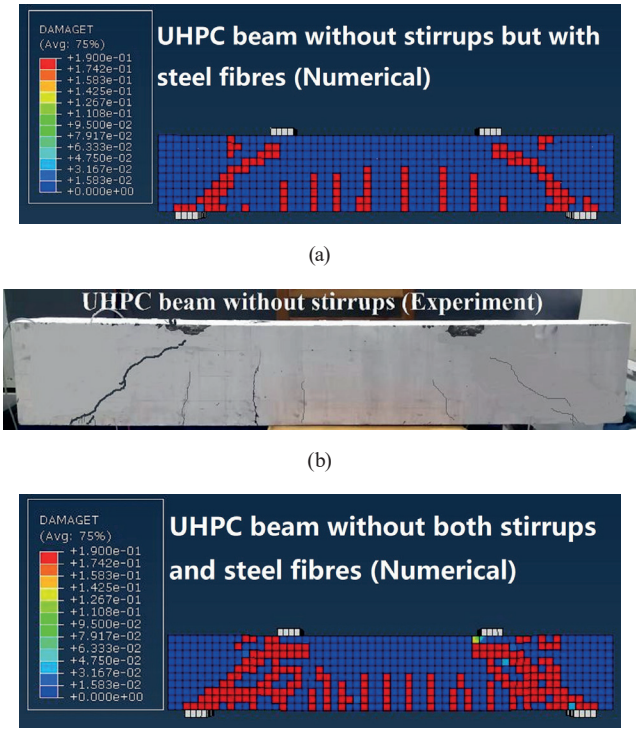

Fig. 12 (a) Crack pattern of UHPC beam without stirrups but with steel fibers (Numerical), (b) Crack pattern of UHPC beam without stirrups (Experiment), (c) Crack pattern of UHPC beam without both stirrups and steel fibers (Numerical)

4.4 Load-midspan displacement behavior of the UHPC beams

The relationship between load and midspan displacement of both the UHPC beam with stirrups and that without stirrups based on Fig. 13 has both linear stage and non-linear stage similar to the research report of Aziz and Ali [18]; and this relationship has the same trend for both experiments and numerical simulations (i.e., numerical beam model with and without steel fibers). The linear stage is the elastic loading stage of the beam below the cracking load where no crack has appeared in the beam (0 to P). The non-linear stage is the inelastic loading stage of the beam after the formation of the first flexural crack; and this stage has three phases which are common in load-midspan displacement of UHPC beams [39, 40]. The first phase is the post-cracking phase (from P to T) where more cracks developed and increased in length and width in the UHPC beam until the tensile steel reinforcement started yielding (point T). The second phase is the plastic deformation phase (from T to U) where the beam continued to bear the load till its ultimate load (point U). The third phase of the beam's inelastic phase is the strain softening phase (from U to F) where it finally failed at point F. Fig. 13 also showed that increase in applied load also leads to increase in midspan

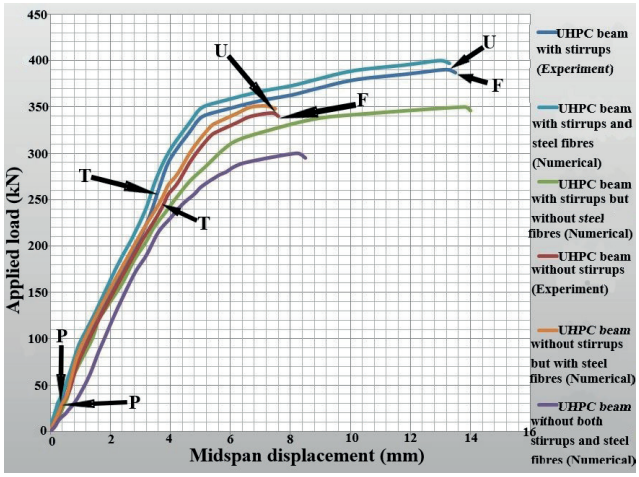

Fig. 13 Applied load-midspan displacement of the UHPC beams

displacement of the beam in agreement with Magureanu et al. [41]; as the experimental midspan displacement of the UHPC beam with stirrups at cracking and ultimate load of 35 and 390.3 kN was 0.4 and 13.2 mm, respectively. The midspan displacement at cracking and ultimate load of 39 and 400 kN was 0.35 and 13.0 mm, respectively for the numerically simulated UHPC beam with stirrups and steel fibers; while the numerically simulated UHPC beam with stirrups but without steel fibers has midspan displacement of 0.55 and 13.8 mm at cracking and ultimate load of 30 and 350 kN, respectively. Analysis of the shear capacity of the UHPC beam with stirrups at ultimate load phase reveals that the numerically simulated beam without steel fibers has about 10.3% shear strength reduction when compared with the experimental beam; while the numerically simulated beam with steel fibers is only 2.5% higher in shear strength than the experimental beam at ultimate load phase. This analysis shows that the incorporation of steel fibers in the UHPC beam with stirrups improves its shear resistance by about 13% and it also reveals that the ultimate load of the experimental beam has better correlation with the numerically simulated beam containing steel fibers than the numerically simulated beam without steel fibers.

As can be seen in Fig. 13 for the UHPC beam without stirrups, the cracking and ultimate load of 33.5 and 343.5 kN for the experimental beam resulted in midspan displacement of 0.7 and 7.4 mm, respectively; the cracking and ultimate load of 36 and 351 kN for the numerically simulated beam without stirrups but with steel fibers resulted in midspan displacement of 0.55 and 7.2 mm, respectively; and the cracking and ultimate load of 28.5 and 300 kN for the numerically simulated beam without both stirrups and steel fibers resulted in midspan displacement of 0.9 and 8.5 mm, respectively. The high ultimate strength of the experimental beam and the numerically simulated beam with steel fibers, even with the elimination of stirrups may be due to the bridging effect provided by steel fibers [24]; while the low midspan displacement is indicative of low shear deformation as a result of the beams' high shear stiffness [42]. These results have proved that the ultimate load of the experimental beam has better agreement with the numerically simulated beam with steel fibers than the numerically simulated beam without steel fibers; and the steel fibers also improved the shear resistance of the beam by 17%. Also, even though this beam was made without shear reinforcement, its ultimate strength for experiment and numerical simulation (with steel fibers) was only 12% lower than that made with stirrups. The high ultimate load and low midspan displacement of the UHPC beam without shear reinforcement has revealed that the load carrying capacity of the beam will not be affected for this type of UHPC beam designed without stirrups.

4.5 Ductility evaluation of the UHPC beams

The ductility of the UHPC beams, which can be simply described as its ability to resist deformation as it passes through elastic and plastic phase to failure was evaluated in order to assess the energy absorption capacity of the beam. It was evaluated using deflection ductility index (μ_u) expressed in Eq. (19) as the ratio of deflection at the ultimate load (Δ_u) to deflection at yielding of tensile steel reinforcement (Δ_y).

$$\mu_u = \frac{\Delta_u}{\Delta_y} \tag{19}$$

The ductility index used for this evaluation was chosen based on existing literatures [38, 43, 44] which showed that it gives better estimation of the response of reinforced concrete beams after the yielding of steel reinforcements than when evaluated at peak load. The deflection results used for the evaluation are presented in Table 3.

The ductility index of the UHPC beams as shown in Fig. 14 reveals that the ductility index of the experimental UHPC beam with stirrups was 3.9; that of the numerically simulated UHPC beam with stirrups and steel fibers was 4.0; and that of the numerically simulated UHPC beam with stirrups but without steel fibers was 3.6. In the same way, the ductility index of the experimental UHPC beam without stirrups was 2.0; that of the numerically simulated

Table 3 Deflection of the UHPC beam at tensile steel yielding and at ultimate load

UHPC Beam type	Deflection at tensile steel yielding (mm)	Deflection at ultimate load (mm)
UHPC beam with stirrups (Experiment)	3.4	13.2
UHPC beam with both stirrups and steel fibers (Numerical)	3.3	13.0
UHPC beam with stirrups but without steel fibers (Numerical)	3.8	13.8
UHPC beam without stirrups (Experiment)	3.7	7.4
UHPC beam without stirrups but with steel fibers (Numerical)	3.3	7.2
UHPC beam without both stirrups and steel fibers (Numerical)	4.7	8.5

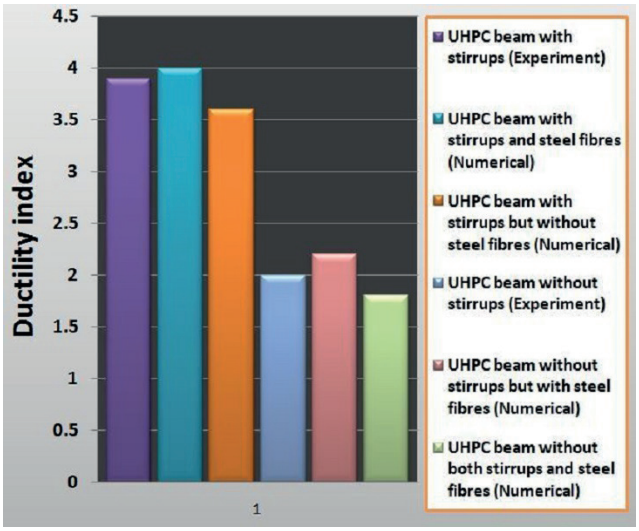

Fig. 14 Ductility index of the UHPC beams

beam without stirrups but with steel fibers was 2.2; and that of the numerically simulated beam without both stirrups and steel fibers was 1.8. The ductility nature of this UHPC beams was also revealed in the slow (and not sudden) increase in the width of the beams' existing cracks after yielding of the tensile steel reinforcements. The ductility reduction of about 48% in the UHPC beam without stirrups can be attributed to the absence of shear reinforcement in the beam; however, it has better ductility when compared with the ductility indices of some studies conducted on high performance concrete and reinforced concrete [45, 46, 44). Further analysis showed that there was 2.6% difference in the ductility index of the experimental beam with stirrups and the numerically simulated beam with stirrups and steel fibers, while 8.3% difference existed between that of the experimental beam with stirrups and the numerically simulated beam with stirrups but without steel fibers. the ductility index of the experimental beam with stirrups is in better agreement with the ductility index of numerically simulated beam with steel fibers than the numerically simulated beam with stirrups but without steel fibers. Moreso, these UHPC beams can be considered to have good ductility when compared to UHPC beams with similar longitudinal reinforcement ratios reported by other researchers [16, 38].

5 Conclusions

In this research work, a simplified technique of modelling steel fibers in a UHPC specimen for the numerical simulation of its properties was proposed. In order to assess the validity of this method, the results on the compressive properties of UHPC cube and the shear behavior of two UHPC beams obtained using this method were compared with the results obtained from experiments and the current method used by researchers for the simulation of UHPC specimens. The following conclusions can be made based on the comparisons between the numerical simulation results and the experimental results:

This method, beside its ability to be directly run in ABAQUS to automatically generate the location and orientation of steel fibers in a UHPC specimen/member, is also very fast, cost-effective, simple to use in studying the effect of % volume of steel fibers and aspect ratio on UHPC specimens/members, and is able to solve the problem associated with previous methods of modeling SFRC where some fibers may be generated and placed outside the specimen's boundary, leading to the discard and regeneration of those fibers. The results of the deformation obtained using this method for the compressed UHPC cube and the two UHPC beams subjected to shear loading agree perfectly with the deformation results of the experiments. Also, the result of the ultimate compression force obtained using this modelling technique has 99.7% agreement with that of the experimental cube. This method improved the shear resistance of the beam with stirrups and that without stirrups by 16 and 14%, respectively at the appearance of the first shear crack; while at the ultimate load phase, the shear resistance of the beam with stirrups and that without stirrups was improved by 13 and 17%, respectively. The ultimate load of the beam with stirrups and that without stirrups obtained using this method has about 97.5 and 97.8% agreement respectively with the ultimate load of the experimental beams, while about 98.5 and 97.3% agreement exist for the same order of aforementioned beams in terms of ultimate midspan displacement. The ductility of the beams also exhibited strong agreement as the ductility of the beam with stirrups using this method has about 97.5% agreement with the experimental beam.

The limitations of this method can be seen in two ways. The first is on the basis that only straight steel fibers can be generated through the algorithm, limiting the method from being used to study the effect of the shape of steel fibers on UHPC specimen’s properties. The second limitation is attributed to the shape of the UHPC specimen; and on this basis, only rectangular specimens can be generated through the algorithm. Although this method is only applicable to straight steel fibers and rectangular specimens, efforts are currently being made through on-going research to modify this method to include the modelling of other shapes of steel fibers as well as cylindrical specimens and structural members with circular shape.

References

[1] ACI 544.1R "State-of-the-Art Report on Fiber Reinforced Concrete", American Concrete Institute, Farmington Hills, MI, USA, 1996. [online] Available at: https://standards.globalspec.com/std/1211937/ACI%20544.1R [Accessed: 01 June 2022]

[2] Singh, P. "Steel fibre reinforced concrete", [pdf] International Journal of Advanced Research in Science and Engineering, 6(01), pp. 382–388, 2017. Available at: http://ijarse.com/images/fullpdf/1485351908_N284_IJARSE.pdf [Accessed: 01 May 2021]

[3] Dinh, H. H. "Sear behaviour of steel fibre reinforced concrete beams without stirrup reinforcement", PhD Dissertation, University of Michigan, 2009.

[4] Naaman, A. E. "Fibre reinforcement for concrete", Concrete International, 7, pp. 21–25, 1987.

[5] Larsen, I. L., Thorstensen, R. T. "The influence of steel fibres on compressive and tensile strength of ultra-high performance concrete: A review", Construction and Building Materials, 256, 119459, 2020.
https://doi.org/10.1016/j.conbuildmat.2020.119459

[6] Kwak, Y.-K., Eberhard, M. O., Kim, W. S., Kim, J. "Shear strength of steel fiber-reinforced concrete beams without stirrups", ACI Structural Journal, 99(4), pp. 530–538, 2002.
https://doi.org/10.14359/12122

[7] ACI Committee 318 "Building code requirements for structural concrete and commentary", [pdf] American Concrete Institute, Farmington Hills, MI, 465, 2008. Available at: http://dl.mycivil.ir/dozanani/ACI/ACI%20318-08%20Building%20Code%20Requirements%20for%20Structural%20Concrete%20(ACI%20318-08)%20and%20Commentary_MyCivil.ir.pdf [Accessed: 01 December 2021]

[8] Zollo, R. F. "Fiber-reinforced concrete: an overview after 30 years of development", Cement and Concrete Composite, 19(2), pp. 107–122, 1997.
https://doi.org/10.1016/S0958-9465(96)00046-7

[9] El-Din, H. K. S., Mohamed, H. A., El-Hak Khater, M. A., Ahmed, S. "Effect of Steel Fibers on Behavior of Ultra High Performance Concrete", [pdf] In: Proceedings of the First Interactive Symposium on UHPC, Des Moines, IA, USA, 2016, pp. 1–10. Available at: https://www.extension.iastate.edu/registration/events/UHPCPapers/UHPC_ID11.pdf [Accessed: 01 April 2021]

[10] Hoang, A. L., Fehling, E. "Influence of steel fiber content and aspect ratio on the uniaxial tensile and compressive behavior of ultra high performance concrete", Construction and Building Materials, 153, pp. 790–806, 2017.
https://doi.org/10.1016/j.conbuildmat.2017.07.130

[11] Ibrahim, M. A., Farhat, M., Issa, M. A., Hasse, J. A. "Effect of material constituents on mechanical and fracture mechanics properties of ultra-high-performance concrete", ACI Materials Journal, 114(3), pp. 453–465, 2017.
https://doi.org/10.14359/51689717

[12] Noghabai, K. "Beams of fiberous concrete in shear and bending: experiment and model", Journal of Structural Engineering, 126(2), pp. 243–251, 2000.
https://doi.org/10.1061/(ASCE)0733-9445(2000)126:2(243)

[13] Oh, S. G., Noguchi, T., Tomosawa, F. "Evaluation of rheological constants of high-fluidity concrete by using the thickness of excess paste", Journal of the Society of Materials Science, 48, pp. 1193–1198, 1999.
https://doi.org/10.2472/jsms.48.1193

[14] Narayanan, R., Darwish, I. Y. S. "Use of steel fiber as shear reinforcement", ACI Structural Journal, 84(3), pp. 216-227, 1987.
https://www.doi.org/10.14359/2654

[15] Garg, V., Bansal, P. P., Sharma, R. "Retrofitting of shear-deficient RC beams using UHP-FRC", Iranian Journal of Science and Technology, Transactions of Civil Engineering, 43, pp. 419–428, 2019.
https://doi.org/10.1007/s40996-019-00241-7

[16] Kodur, V., Solhmirzaei, R., Agrawal, A., Aziz, E. M., Soroushian, P. "Analysis of flexural and shear resistance of ultra-high performance fiber reinforced concrete beams without stirrups", Engineering Structures, 174, pp. 873–884, 2018.
https://doi.org/10.1016/j.engstruct.2018.08.010

[17] Baby, F., Marchand, P., Toutlemonde, F. "Shear behavior of ultra-high performance fiber-reinforced concrete beams II: analysis and design provisions", Journal of Structural Engineering, 140(5), pp. 1–11, 2014.
https://doi.org/10.1061/(ASCE)ST.1943-541X.0000908

[18] Aziz, O. Q., Ali, M. H. "Shear strength and behavior of Ultra-high performance fiber reinforced concrete (UHPC) deep beams without web reinforcement", International Journal of Civil Engineering (IJCE), 2(3), pp. 85–96, 2013.

[19] Xu, Z., Hao, H., Li, H. N. "Mesoscale modelling of fibre reinforced concrete material under compressive impact loading", Construction and Building Materials, 26(1), pp. 274–288, 2012.
https://doi.org/10.1016/j.conbuildmat.2011.06.022

[20] Liang, X., Wu, C. "Meso-scale modelling of steel fibre reinforced concrete with high strength", Construction and Building Materials, 165, pp. 187–198, 2018.
https://doi.org/10.1016/j.conbuildmat.2018.01.028

[21] Fang, Q., Zhang, J. "Three-dimensional modelling of steel fiber reinforced concrete material under intense dynamic loading", Construction and Building Materials, 44, pp. 118–132, 2013.
https://doi.org/10.1016/j.conbuildmat.2013.02.067

[22] Hashim, D. T., Hajezi, F., Lei, V. Y. "Simplified constitutive and damage plasticity models for UHPFRC with different types of fiber", International Journal of Concrete Structures and Materials, 14, 45, 2020.
https://doi.org/10.1186/s40069-020-00418-9

[23] Bahij, S., Adekunle, S. K., Al-Osta, M., Ahmad, S., Al-Dulaijan, S. U., Rahman, M. K. "Numerical investigation of the shear behavior of reinforced ultra-high-performance concrete beams", Structural Concrete, 19(1), pp. 305–317, 2018.
https://doi.org/10.1002/suco.201700062

[24] Solhmirzaei, R., Kodur, V. K. R., Banerji, S. "Shear behavior of ultra-high performance concrete beams without stirrups", International Symposium on Ultra High Performance Concrete, 2(1), 2019.
https://doi.org/10.21838/uhpc.9665

[25] Hussein, L. "Structural behavior of ultra-high performance fibre reinforced concrete composite members", PhD Dissertation, Ryerson University, 2015.

[26] Romualdi, J. P., Mandel, J. A. "Tensile strength of concrete affected by uniformly distributed and closely spaced short lengths of wire reinforcement", Journal Proceedings, 61(6), pp. 657–672, 1964. https://doi.org/10.14359/7801

[27] Blueberry Blackcurrant "纤维混凝土的Abaqus参数化建模 (Abaqus Parametric modeling of fiber concrete)", Abaqus Civil Engineering Case Analysis in Building Structure Simulation, Architectural Structure Design, 2021. [online] Available at: https://zhuanlan.zhihu.com/p/383621614 [Accessed 30 November 2021] (in Chinese)

[28] BS EN 12390-3 "Method for Determination of compressive strength of concrete", British Standard Institution, London, UK, 2009.

[29] EN 1992-1-1 "Design of concrete structures-part 1-1: general rules and rules for buildings", European Committee for Standardization, Brussels, Belgium, 2004.

[30] BS 8110-1 "Structural use of concrete-part 1: code of practice for design and construction", British Standard Institution, London, UK, 1997.

[31] GB/T 50152-2012 "Standard for test methods for concrete structures", National Standard of the People's Republic of China, Beijing, China, 2012.

[32] Funk, J. E., Dinger, D. R. "Predictive process control of crowded particulate suspensions, applied to ceramic manufacturing", Kluwer Academic Publishers, 1994. ISBN 978-0-7923-9409-9 https://doi.org/10.1007/978-1-4615-3118-0

[33] Lubliner, J., Oliver, J., Oller, S., Oñate, E. "A plastic-damage model for concrete", International Journal of Solids and Structures, 25(3), pp. 299–326, 1989. https://doi.org/10.1016/0020-7683(89)90050-4

[34] T/CBMF 37-2018 (2018) "Fundamental characteristics and test methods of ultra-high performance concrete", Standard of China Building Materials Association, Beijing, China, 2009. [online] Available at: https://www.doc88.com/p-58139740621068.html (in Chinese)

[35] CECS13-2009 (2009) "Standard test method for fibre reinforced concrete", Standard of China Engineering Construction Association, Beijing, China, 2009. [online] Available at: https://www.doc88.com/p-91773113625122.html (in Chinese)

[36] Birtel, V. Mark, P. "Parameterised finite element modelling of RC beam shear failure", In: Proceedings of 2006 ABAQUS Users' Conference, Providence, RI, USA, 2006, pp. 95–108.

[37] ASTM C39/C39M "Standard test method for compressive strength of cylindrical concrete specimens", American Society for Testing and Materials International, West Conshohocken, PA, USA, 2014.

[38] Yang, I. H., Joh, C., Kim, B.-S. "Structural behavior of ultra-high performance concrete beams subjected to bending", Engineering Structures, 32(11), pp. 3478–3487, 2010. https://doi.org/10.1016/J.ENGSTRUCT.2010.07.017

[39] Hassan, A. M. T., Jones, S. W., Mahmud, G. H. "Experimental test methods to determine the uniaxial tensile and compressive behaviour of ultra-high performance fibre reinforced concrete (UHPFRC)", Construction and Building Materials, 37, pp. 874–882, 2012. https://doi.org/10.1016/j.conbuildmat.2012.04.030

[40] Fehling, E., Bunje, K., Leutbecher, T. "Design relevant properties of hardened ultra-high performance concrete", presented at Proceedings of the International Symposium on Ultra-High Performance Concrete, Kassel, Germany, Sep, 13–15, 2004.

[41] Magureanu, C., Sosa, I., Negrutiu, C., Heghes, B. "Bending and shear behavior of ultra-high performance fiber reinforced concrete", In: International Conference on High Performance and Optimum Structures and Materials Encompassing Shock and Impact Loading, High Performance Structures and Materials V, Lisbon, Portugal, 2010, pp. 79–89. https://doi.org/10.2495/HPSM100081

[42] Ueda, T., Sato, Y., Ito, T., Nishizono, K. "Shear deformation of reinforced concrete beam", Journal of Materials, Concrete Structures and Pavements, 711, pp. 205–215, 2002. https://doi.org/10.2208/jscej.2002.711_205

[43] AFGC-Association Française de Génie Civil "French interim recommendations of ultra-high performance fibre reinforced concrete (UHPFRC)", French Association of Civil Engineers, Paris, France, 2002.

[44] Islam, M. S. "Shear capacity and flexural ductility of reinforced high- and normal-strength concrete beams", MPhil Thesis, The University of Hong Kong, 1996. https://doi.org/10.5353/th_b3121444

[45] Kim, T.-K., Park, J.-S. "Evaluation of the performance and ductility index of concrete structures using advanced composite material strengthening methods", Polymers, 13(23), 4239, 2021. https://doi.org/10.3390/polym13234239

[46] Bernardo, L. F. A., Lopes, S. M. R. "Neutral axis depth versus flexural ductility in high strength concrete beams", Journal of Structural Engineering, 130(3), pp. 452–459, 2004. https://doi.org/10.1061/(ASCE)0733-9445(2004)130:3(452)